Polymer 51 (2010) 3762–3773

Contents lists available at ScienceDirect

Polymer

journal homepage: www.elsevier.com/locate/polymer

Stress - Optical behavior of Poly(*m*-xylylenediamine adipamide) (Nylon MXD6): Influence of molecular weight

Sylvain Seif, Miko Cakmak*

Polymer Engineering Institute, College of Polymer Engineering and Polymer Science, University of Akron, Akron, OH 44325, United States

ARTICLE INFO

Article history:
Received 23 February 2010
Received in revised form
2 June 2010
Accepted 7 June 2010
Available online 12 June 2010

Keywords:
Stress and Strain optical Behavior
MXD6

ABSTRACT

The effect of molecular weight and rubbery state uniaxial stretching conditions on the mechano-optical behavior of Poly(*m*-xylylenediamine adipamide) (Nylon MXD6) films was investigated using a real time spectral birefringence stretching machine. The stress optical behavior exhibits a multi stage behavior that depends on process conditions as well as molecular weight. At low stretching temperatures and high rates the stress optical behavior was found to start with an initial glassy photo elastic behavior. Decreasing stretching rate or increasing processing temperature was found to eliminate this glassy photoelastic regime leading to the observation of a linear initial stress optical behavior past a temperature of 95 °C (T_{ll}). The stress optical constant (SOC) was about the same for both M.W. materials stretched at temperatures past T_{ll}, at 2.7 GPa^{-1} for HPA6 and 2.61 GPa^{-1} for LPA6. Following this initial regime, the behavior is controlled by the competition between orientation and relaxation during deformation. If the chain orientation relaxation is not suppressed by increasing the stretching rate and/or the molecular weight or by decreasing temperature, the material strain crystallizes.

1. Introduction

Poly(*m*-xylylenediamine adipamide)(MXD6) is an aromatic polyamide produced by monomers

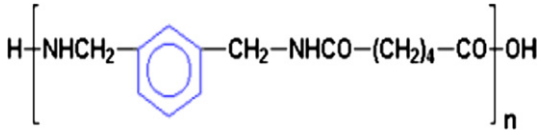

polymerization of *m*-xylylenediamine and adipic acid (hexan-1,6-dioic acid) [1]. It is well known for its superior gas barrier properties. This material exhibits a slow crystallization character and is easily quenched into the glassy state, closely resembling the behavior of PET [2]. Because of the latter behavior it shows good processability in thermoforming, stretch blow molding and tenter film biaxial stretching operations [3]. Hence, Nylon MXD6 is widely used in the production of films, sheets and rigid containers as a new type of high gas barrier resin [4]. For instance, Nylon MXD6 is currently being used for PET bottle applications, both as a barrier layer in multilayer bottles or as a single layer blended with PET [5]. Owing to its processability, recyclability, moderate adhesion to PET layers and total cost, Nylon MXD6 is well suited as a high barrier material in PET bottle applications for tea, juice, carbonated soft drinks or beer [4]. During the fabrication of these products, the quenched amorphous polymer is oriented in the temperature range ($T_g < T_p < T_{cc}$) where it behaves rubbery and where thermal crystallization practically does not occur due to an extremely long half time of crystallization.

In immiscible blends containing a minor component of MXD6, orientation has been shown to transform dispersed spherical MXD6 domains into platelets oriented in the plane of the film [6]. The formation of this disk-like phase increases the tortuosity of the diffusion pathway arising from the high aspect ratio MXD6 platelets, thus leading to increased barrier properties [6].

Upon stretching in the rubbery state from amorphous precursors, polymer chains orient and after a certain degree of orientation is reached, they may undergo stress induced crystallization resulting in mechanical strain hardening [7,8]. As the level of crystallinity increases in a sample, a crystalline network develops and stabilizes the bulk material with respect to properties such as shrinkage and heat distortion [9]. The presence of stress induced crystallization leads to “self-leveling” in polymer films as the thinned portions of the material stop deforming and thicker portions are deformed to the same level, yielding a uniform thickness distribution [10]. If this mechanism is absent or delayed to high strain levels, the resulting product would contain commercially undesirable thickness distributions. If one can attain early onset of stress induced crystallization, the finished product would have a lower thickness distribution [11], lower gas diffusion

* Corresponding author.
E-mail address: cakmak@uakron.edu (M. Cakmak).

0032-3861/$ – see front matter © 2010 Elsevier Ltd. All rights reserved.
doi:10.1016/j.polymer.2010.06.014

characteristics [6], better thermal stability [11], mechanical properties [7,8], and enhanced optical clarity through amplified stress enhanced crystal nucleation [12,13]. In the early stage of deformation stress has been found to linearly correlate with birefringence, following the stress optical rule (SOR)

$$\Delta n = C\sigma \tag{1}$$

This relationship has been used extensively in polymeric melts but has also been shown to be valid for amorphous polymers at low to moderate stress levels [14,15]. Here C is the stress optical constant. Beyond low to moderate stress levels, however, a deviation from linear SOR occurs. For instance, if stress induced crystallization occurs in a material, a positive deviation from linearity, associated with a Regime II behavior was observed [6–8,16,17]. Finally, at high stress levels non-Gaussian segmental distribution is present as the chains approach their finite extensibilities and a negative deviation from linearity (Regime III behavior) occurs with stress increasing while birefringence approaches a plateau [7,18,19]. In the past [7,8], it has been shown that utilization of fast deformation rates and lower temperatures prevents the stress induced crystallization particularly when the polymers possess high molecular weight and consequent high entanglement density. Under these conditions Regime I–IIIa behavior is observed where the IIIa regime slope negatively deviates from the Regime I. The structures of such materials were found to possess substantial preferred chain orientation and translational disorder along the stretching direction.

When stretched near their glass transition temperatures, however, polymers may initially exhibit a photoelastic glassy behavior with stress increasing rapidly while birefringence increases slowly [20–22]. This glassy behavior disappears at some temperature T_{ll}, which has been defined as a temperature at which the material changes from a "fixed liquid" state to a "true liquid" state on the basis of rheological behavior [23,24]. Murthy [23] describes a model of the liquid regime consisting of dynamic clusters (α regions) surrounded by "liquid-like" β regions. According to this model, the part of the polymer chain involved in the cooperatively rearranging α region can be viewed as a "segment". With an increase of temperature, the "surface melting" of these clusters starts at T_g, with the result that the number of repeat units that go into the surrounding liquid increases and the size of the segment that is involved in the cooperative α process decreases. In other words, the strength of the β process increases at the cost of the α process. Boyer and Frenkel [25,26] have also treated the temperature T_{ll} as that above which complete "melting" of clusters or segments takes place. They describe the existence of "segmental crystals" at temperatures below T_{ll} that prevent the material from behaving as a true liquid as they act as additional junction points in a physical network composed of entanglements. As soon as these preexisting "segmental crystals" disintegrate beyond the T_{ll}, the material starts showing rubbery deformation with the Regime I following the stress optical rule and the strain-optical behavior after this transition becomes completely non-linear indicating no inherent network holding the material anymore. The authors have also shown that the liquid–liquid transition is considered a relaxation and not a thermodynamic transition as it is frequency-dependent.

The Poisson's ratio, ν, is defined as the relationship between the strain produced by a tensile force and the resulting contraction that occurs in directions perpendicular to it [27,28].

The calculation of Poisson's ratio is hence taken as follows [27]:

$$\nu = -\frac{\varepsilon_{\text{trans}}}{\varepsilon_{\text{axial}}} = -\frac{\varepsilon_x}{\varepsilon_y} \tag{2}$$

where $\varepsilon_{\text{trans}}$ is the transverse direction (TD) strain and $\varepsilon_{\text{axial}}$ is the machine direction (MD) strain.

In an isotropic material the range of Poisson's ratio is given by $-1 \le \nu \le 0.5$. Although the Poisson's ratio is very close to 0.5 for an incompressible material, a Poisson's ratio of 0.5 corresponds to an infinite bulk modulus and is thus never attained in practice [28].

Very few researchers have studied the effects of strain on the evolution of Poisson's ratio; in fact, most studies on Poisson's ratio literature consider only one value of Poisson's ratio, when the deformation is infinitesimally small. Furthermore, most of the other Poisson's ratio studies done to date [27–33] deal only with Poisson's ratio changes under small deformation levels, discovering that Poisson's ratio has a non-linear dependence on axial strain. Equation (2), however, has only limited value for materials since ν thus defined is not constant at large strains. Smith [33] addressed this issue by defining Poisson's ratio in terms of the logarithmic or Hencky strains:

$$\nu = -\frac{d\ln\frac{V}{V_0}}{2\ln\lambda_1} + \frac{1}{2} = -\frac{d\ln\lambda_2}{d\ln\lambda_1} \tag{3}$$

whereby λ_1, λ_2 and λ_3 are the extension/contraction ratios in the machine, transverse and normal directions, respectively. This definition has several advantages in that ν is independent of strain for constant volume and at the same time $\nu = 0.5$ is still associated with incompressibility.

Choi and Lakes [29] observed an increase in Poisson's ratio at small strain levels for various conventional and re-entrant polymer cellular solids (foams). They explained this behavior by using the fact that the Poisson's ratio is affected by the competition between the Young's modulus and the Bulk modulus of the material, by the following relationship [29]:

$$\nu(t) = \frac{1}{2} - \frac{E(t)}{6B(t)} \tag{4}$$

The authors stated that for polymeric materials, when the Young's modulus E relaxes much more than the Bulk modulus B during stretching, Poisson's ratio increases monotonically with time. Wilson et al. [30] and later on Ma et al. [32] have also observed similar Poisson's ratio increases at low strain levels in PET and PEN film, respectively. However, all of these authors performed their studies at room temperature conditions, whereby the polymers are deformed in the glassy state. Kugler et al. [31] measured Poisson's ratio in a series of filled elastomers using a novel optoelectronic system. They observed sharp decreases of Poisson's ratio with strain, relating this to binder/filler debonding or cavitation which leads to a high rate of vacuole formation around the embedded particles and henceforth a significant increase in volume that gives rise to large negative slopes, according to equation (3).

Controlling material properties through control of orientation and phase development require a clear understanding of the effects of molecular weight and processing conditions, including temperature, rate and extent of stretching, on stress optical relationships during the deformation process. During fast deformation processes, structural transitions may occur quickly and are very difficult to explain using traditional offline techniques. Hence, in order to elucidate the details of the molecular mechanisms that rapidly change during processing, real time birefringence/true mechanical behavior measurement systems must be employed. In this study, a uniaxial stretching instrument equipped with a unique on-line measurement device is utilized in order to monitor the structural changes that occur during the deformation/relaxation processes of Nylon MXD6 "real time".

In this paper, the effects of molecular weight and processing conditions on the variation of Poisson's ratio during large deformation "rubbery-state" stretching of Nylon MXD6 are investigated in great detail. This paper also seeks to present a comprehensive mechano-optical study of the deformation of two different M.W. Nylon MXD6 grades stretched in the rubbery state to various extension levels under differing rates and temperatures, using a well-equipped uniaxial stretching device that allows for the real time simultaneous recording of true stress, Hencky strain and optical retardation [7,8]. Furthermore, this study utilizes offline wide angle X-ray diffraction (WAXD) methods in order to reveal the structural mechanisms that take place in the material during uniaxial deformation, as affected by molecular weight and processing conditions.

2. Experimental section

2.1. Materials and film preparation

Two different grades of Nylon MXD6 material, Nylon MXD6 6001 and Nylon MXD6 6007, produced by Mitsubishi Gas Chemical, Inc. are used for this study. ATR FTIR (A Nicolet Nexus-870 Fourier transform IR) tests taken on melt cast samples of Nylon MXD6 confirm the chemical structure shown above (Fig. 1). The number-average molecular weight (M_N) of the 6001 grade was 16,200 g/mol, while that of the 6007 grade was 25,920 g/mol[2]. After drying to less than 0.1% moisture content, the pellets were provided in moisture-proof bags. Thus, no pre-drying was needed immediately before processing. The melt casting was carried out using a Prodex single screw extruder attached to an 8" wide sheet casting die. The casting conditions employed are shown in Table 1. In order to prevent moisture uptake during the feeding stage, the pellets were fed under a nitrogen gas blanket inside of the hopper. The films ranged between 0.25 mm and 0.28 mm in thickness, implying relative uniformity in the melt casting process.

2.2. On-line birefringence and stress–strain measurements

A uniaxial stretching instrument, described in detail elsewhere [8,34,35] was developed in our group to simultaneously determine the true mechanical and optical properties of Nylon MXD6 films during the deformation process. This machine is essentially composed of three parts: the uniaxial stretching device with an environmental chamber, a spectral birefringence system, and

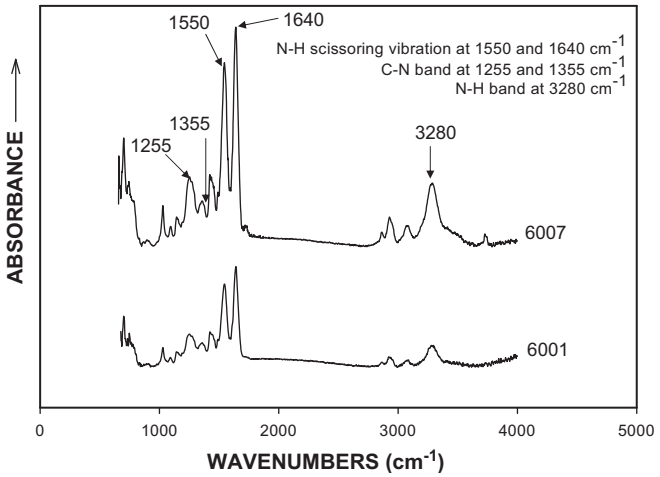

Fig. 1. IR spectra (ATR mode) of as received Low molecular weight (6001) and high molecular weight (6007) Nylon MXD5 films.

Table 1
Film casting conditions employed for Nylon MXD6 material.

Feed temperature (Zone 1)	255° C
Compression section temperature (Zone 2)	260° C
Metering temperature (Zone 3)	265° C
Adapter temperature	265° C
Die temperature	265° C
Chill roll temperature	66 °C
Screw speed	33 rpm
Take-up speed	100 fpm
Die gap thickness	0.4 mm

a laser-based width measurement system. Real time measurements of sample width, optical retardation, force and elongation are recorded simultaneously using this machine. Assuming (1) simple extension and (2) incompressibility, the time variation of the local thickness is calculated, and hence local true stresses and local true strains are calculated using:

$$\text{True strain}(\varepsilon_t) = \frac{L_t}{L_0} - 1 = \left(\frac{W_0}{W_t}\right)^2 \tag{5}$$

$$\text{True stress} = \frac{F_t}{(W_t D_t)} = \frac{F_t}{\left[\left(\frac{W_t}{W_0}\right) D_0\right]} \tag{6}$$

where W_t is the real time width of the film, W_0 is the initial width of the film, L_0 is the initial length of the film, L_t is the real time length of the film, F_t is the time variation of force, D_0 is the initial film thickness and D_t is the real time film thickness calculated using uniaxial symmetry:

$$D_t = \left(\frac{W_t}{W_0}\right) D_0 \tag{7}$$

From the true strain, the Hencky strain is then calculated as follows:

$$\text{Hencky strain } (\varepsilon_H) = \ln\left(\frac{L_t}{L_0}\right) = \ln(\varepsilon_t + 1) \tag{8}$$

Since the sample width is continuously measured during the deformation process and the development of crystallinity is concentrated near the end of the stretching, the film is assumed to exhibit incompressibility [8].

Film specimens that were used in the uniaxial stretching machine consisted of a dumbbell-shape with the following dimensions: 75 mm long, 40 mm wide and 30 mm wide in the narrowest region, as shown in Fig. 2. The benefits of using dumbbell-shaped specimens are that they ensure that measurements are taken at the region experiencing almost all of the deformation, or at the narrowest region of the sample. The samples were clamped and fixed in the arms of the uniaxial stretching machine inside the environmental oven. The distance between the clamps was approximately 30 mm. Prior to the beginning of each test, a thermocouple touching the film surface was used in order to ensure that the film has reached the desired temperature. This constituted a pre-heating time of approximately 15 min for the film to thermally equilibrate in the oven to the stretching temperature employed. After the samples were stretched at the desired conditions, they were cooled at room temperature prior to removal from the clamps.

2.3. DSC testing

The thermal properties of Nylon MXD6 films were measured using a universal 2920 MDSC V2.6A TA Instruments DSC. The

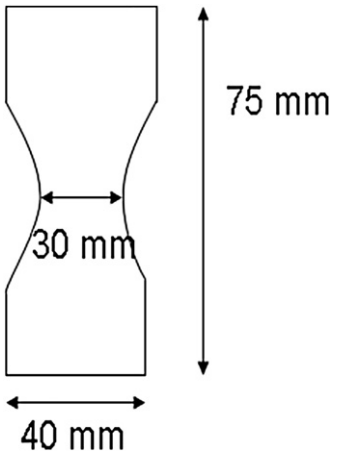

Fig. 2. An unstretched film sample before loading in the environmental chamber of the uniaxial stretching device.

samples of roughly 5–10 mg were crimped in aluminum pans and were then scanned at a heating rate of 10 °C/min under a dry nitrogen atmosphere. The TA Universal Analysis software was used to analyze the DSC results. The reported transition temperatures, T_{cc} and T_m, refer to the peak maximum positions.

2.4. WAXD measurements

The WAXD experiments used in this study were performed using a Bruker AXS generator equipped with a copper target tube and a two-dimensional detector. The generator was operated at 40 kV and 40 mA with a beam monochromized to Cu Kα radiation ($\lambda = 1.54$Å). A customary detector-to-sample distance of 15 cm was used, with 2θ set to 20° and χ set to 45°. One-quadrant WAXD patterns of uniaxially oriented samples were obtained.

2.5. Poisson's ratio studies

A robust on-line true-stress–strain-electrical conductivity–thermal effect monitoring uniaxial stretching system has been developed in our group [36]. The system allows for the simultaneous monitoring of true strain and stresses as well as birefringence during processing. In this research, the machine was utilized in order to measure the true mechanical properties of both M.W. Nylon MXD6 grades under varying rates and isothermal conditions, with particular focus on the ($T_g < T_{operation} < T_{cc}$) range.

In these measurements, a high speed video capture system was employed to obtain strains in the machine and transverse directions based on a pre-painted dot matrix pattern, as this allowed for the assessment of Poisson's ratio as influenced by the processing conditions.

Based on laser-based width measurement data and the uniaxial symmetry assumption, the instantaneous thickness was calculated from knowledge of the initial sample width and initial sample thickness. With only this data, however, the strain measured in the machine direction may be affected if the Poisson's ratio is different from 0.5. In order to address this issue, a high speed CCD camera was implemented to directly measure MD and TD strains based on a pre-painted dot matrix pattern on the surface of the sample.

The unstretched sample geometry consisted of a dumbbell-shape having an initial length of approximately 82.5 mm and an initial width of approximately 42 mm in the center of the sample. The sample thickness ranged from 0.25 to 0.28 mm, and the distance between the clamps was approximately 42 mm. A pre-heating time of approximately 15 min was used for the film to thermally equilibrate in the oven to the stretching temperature employed, as validated by Pyrometer data. Fig. 3 depicts a schematic of the region of interest of a CCD image, the dot pattern matrix on the polymer film sample and the geometry of an unstretched sample.

3. Results and discussion

3.1. Thermal properties of nylon MXD6

The glass transition temperatures (T_g), cold crystallization temperatures (T_{cc}) and melt temperatures (T_m) of as-cast, low and high M.W. Nylon MXD6 film samples are shown in the DSC plots of Fig. 5. From these values, it is evident that the material is well within the rubbery state in the temperature range between 80 and 105 °C. Hence, a stretching window of 80–105 °C was chosen in uniaxial stretching tests, as depicted in Fig. 4.

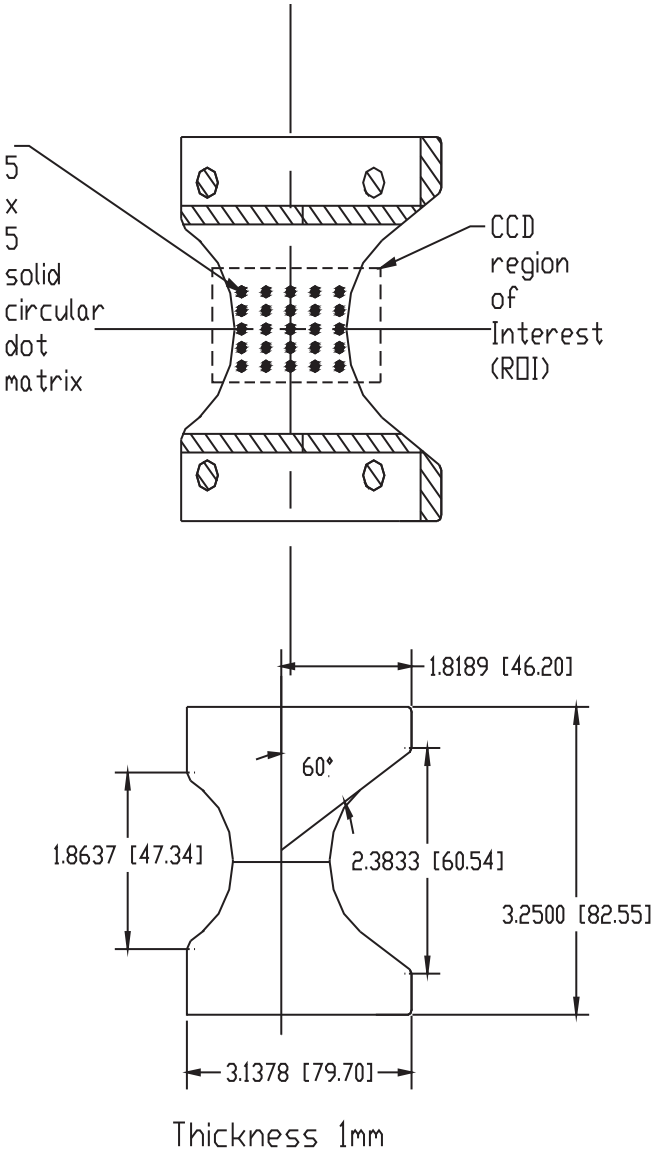

Fig. 3. The geometry of an unstretched polymer sample before loading in the environmental chamber of the K1-machine36.

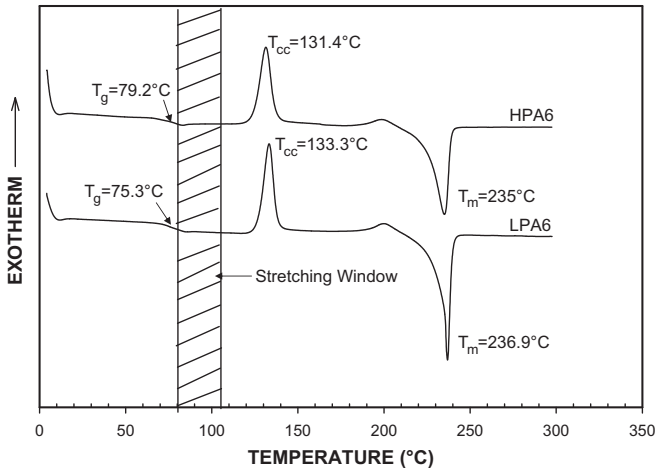

Fig. 4. DSC thermograms of as-cast low and high M.W. Nylon MXD6 film.

From the DSC scans, one can note that the T_g, T_{cc} and T_m values for the as-cast samples are not significantly affected by the molecular weight.

3.2. Mechanical behavior

Fig. 5a and b depict the true stress–Hencky strain behavior of films stretched at various temperatures and at a rate of 67%/min to a global stretch ratio of 6×, or until fracture occurs. Just above the glass transition temperature (80, 85 °C), Nylon MXD6 deforms homogeneously up to a critical stress level, after which it exhibits yielding. Increasing stretching temperatures reduces the yield stress until it completely disappears at temperatures between 85 °C and 90 °C.

This mechanical behavior represents the real mechanical behavior at the stationary midpoint of the sample where the optical retardation and thickness are continuously monitored. Increasing the stretching temperature also increases the strain at which strain hardening occurs. This strain hardening disappears in LPA6 stretched at 100 °C and HPA6 stretched at 105 °C. Under these conditions, the material exhibits no strain hardening or "taffy-pull" characteristics. As we will show below, under these conditions, neither strain induced crystallization nor thermal induced crystallization occurs.

Fig. 6a and b summarize the effects of M.W. and stretch rate (at 90 °C) and stretching temperature (at 67%/min) on the strains at the onset of strain hardening. For the same rates, higher M.W. samples were observed to strain harden at lower critical strains. The strain hardening mechanism is delayed to higher Hencky strains as the rate is lowered. Under the same thermal treatment, HPA6 strain hardens at lower strains than LPA6 as expected from the differences in entanglement density between these two samples (Fig. 6b).

3.3. Poisson's ratio

Fig. 7a and b depict the effect of stretch rate on the evolution of Poisson's ratio with machine direction (MD) Hencky strain for LPA6 and HPA6 samples stretched at 90 °C, and show how the Poisson's ratio vs. MD Hencky strain plots are affected by the stress–strain behavior. Poisson's ratio initially increases for all low molecular weight samples and for high molecular weight MXD6 stretched at low rates. High MW samples that are stretched at intermediate to high rates show slight glassy behavior at early stages of deformation and the Poisson's ratio does not show initial increase but rather starts high and continues to decrease. Choi and Lakes [29] suggested that the Young's modulus E relaxes much more than the Bulk modulus B during stretching as a result of more molecular relaxation during the orientation/relaxation competition, causing the Poisson's ratio to increase monotonically with strain according to equation (4). Interestingly, from Fig. 7b one can see that the slope of the initial Poisson's ratio rise with MD strain increases as the stretch rate decreases for LPA6, as a result of higher chain relaxation which leads to a larger difference between the MD and TD Hencky strains ($\ln \lambda_1$ and $\ln \lambda_2$ terms in equation (3)) over time.

In all cases, beyond the onset of strain hardening (indicated by black circle symbols in Fig. 7) the Poisson's ratio linearly decreases with MD Hencky strain. As expected, increasing the stretching rates decreases the strain at the onset of strain hardening. Fig. 8a and b depict the effect of temperature on the evolution of Poisson's ratio with machine direction (MD) Hencky strain for LPA6 and HPA6 samples stretched at 67%/min. These graphs clearly depict that in samples in which higher chain relaxation takes place due to either lower molecular weight or higher temperatures (more fluidity), an initial rise of Poisson's ratio with MD strain is observed.

3.4. Mechano-optical behavior

3.4.1. Effect of temperature

3.4.1.1. Stress optical behavior. When a polymer of slow crystallization character (PLA, PET, PEN) is stretched from amorphous precursors in at or above T_g they exhibit a common stress optical behavior [7,8,11]. This generalized behavior is graphically shown in

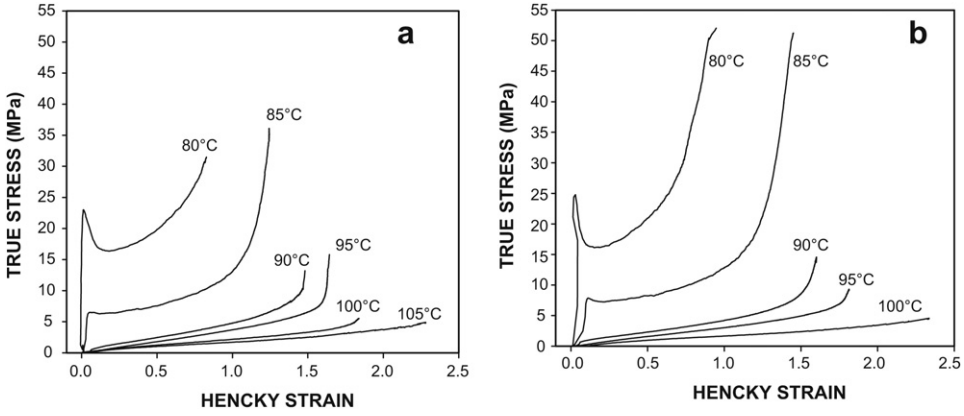

Fig. 5. True stress–Hencky strain behavior of (a) HPA6 and (b) LPA6 films stretched at various temperatures and a rate of 66.7%/min.

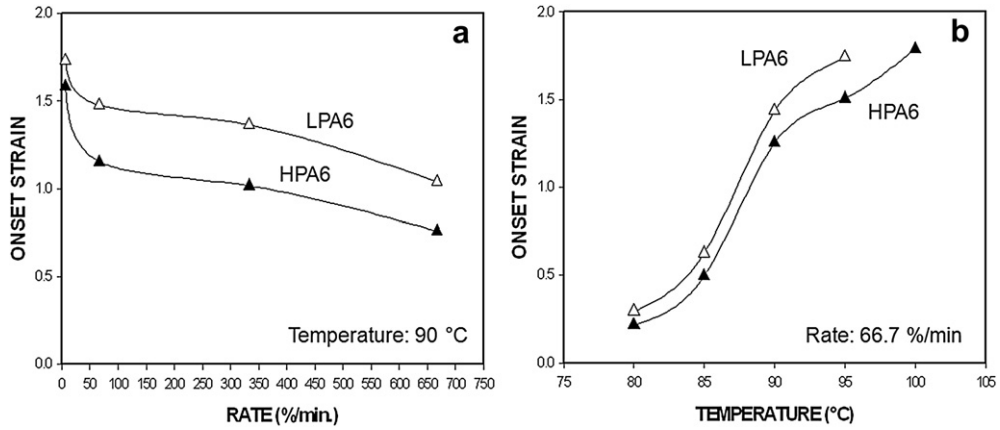

Fig. 6. Effects of (a) M.W. and stretch rate and (b) M.W. and stretching temperature on the Hencky strains at the onset of strain hardening for Nylon MXD6 samples.

Fig. 9. When deformation occurs at high enough temperatures or conditions in which chain relaxation takes place, a Regime I–II–IIIc behavior is observed whereby the material undergoes strain crystallization in the transition from Regime I to II.

When stretched at temperatures just above glass transition and below T_{II}, the material does not strain crystallize and only a Regime I–IIIa behavior, preceded by a photoelastic glassy behavior, with birefringence increasing very little with large increases in stress, is present [37].

The birefringence vs. stress behaviors of LPA6 and HPA6 samples stretched at 67%/min and various temperatures to a global stretch ratio of 6×, or until fracture, are depicted in Fig. 10a and b. For both M.W. grades, a glassy component occurs at lower temperatures and recedes with increasing temperature, until disappearing altogether at 95 °C. For all samples in which the photoelastic glassy behavior is seen, a Regime I–IIIa stress optical behavior follows, with the occurrence of a birefringence increase with stress relaxation due to yielding before Regime I behavior begins. The difference between the behaviors of the two M.W. grades is that the HPA6 material exhibits Regime II at 95 °C and higher temperatures, whereas the LPA6 material continues to show Regime I–IIIa behavior even at the highest stretching temperature (100 °C) before the thermal crystallization begins to be significant.

When HPA6 is stretched at 95 °C, a Regime I–II–IIIc behavior takes place. This is because the high entanglement densities associated with a high molecular weight material alongside relaxation promoted at high temperatures and low stretching rates tend to convert an oriented amorphous structure into a stress induced crystalline structure. The fact that there is a very slow increase of birefringence with stress (Regime IIIc behavior) after the completion of Regime II is due to the long-range tightly connected physical network that forms when stress induced crystallization takes place. This network "locks" the chain structure in place, slowing down the development of further orientation until a birefringence plateau is eventually reached. At 100 °C and above, the Regime III is not reached even when the samples are stretched as much as 6×. This coincides with the fact that very little (at 100 °C) to no (at 105 °C) strain hardening occurs at these elevated temperatures, making the material exhibit "taffy-pull" character as shown in Fig. 5. Of particular interest is the behavior of the material at 105 °C, whereby the birefringence relaxes with increasing stress and a negative deviation from the linearity of the SOR occurs before Regime II is reached. The reasoning behind this is that this temperature is high enough so that relaxation process dominates the orientation while no thermal or stress induced crystallization takes place.

3.4.1.2. Strain-optical behavior. Fig. 11a and b display graphs of the strain-optical behaviors of LPA6 and HPA6 samples stretched at 67%/min. and various temperatures. Linear or near-linear strain-optical behavior is observed under the conditions where the Regime II is absent, whereas a highly non-linear large deformation behavior, where birefringence increases dramatically with small increases in strain, is observed at conditions where the Regime II is present. As Fig. 11b indicates, non-linearity occurs during the late stages of deformation in the strain-optical plot of LPA6 stretched at 95 °C and 67%/min., although the slope of this non-linear region is substantially lower than that of HPA6 stretched under identical conditions.

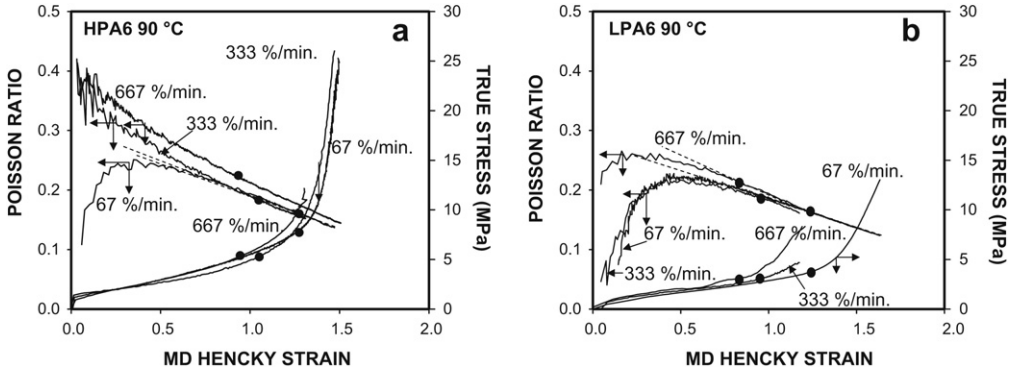

Fig. 7. Effect of stretch rate on Poisson ratio vs. MD Hencky strain and true stress vs. MD Hencky strain behaviors of Nylon MXD6 film.

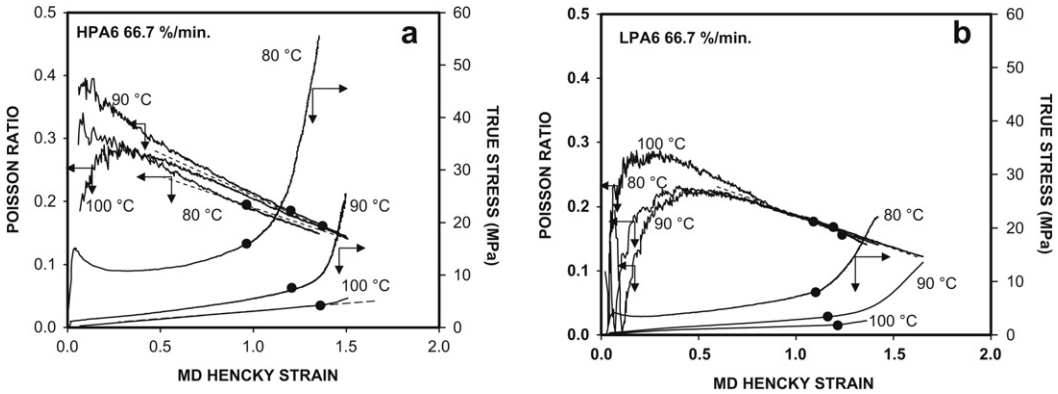

Fig. 8. Effect of temperature on Poisson ratio vs. MD Hencky strain and true stress vs. MD Hencky strain behaviors of (a) HPA6 and (b) LPA6 film samples stretched at 66.7%/min.

3.5. Effect of rate

3.5.1. Stress optical behavior

3.5.1.1. HPA6. Fig. 12 depicts the birefringence vs. stress behavior of HPA6 as influenced by stretch rate and temperature.

At 85 °C, with the decrease in stretching rate the initial glassy behavior decreases approaching Regime I–IIIa stress optical behavior. At stretching temperature of 90 °C, high rates of stretching exhibit the behavior observed at lower temperature and decrease of rate reduces the initial glassy behavior. At very low rate of 6.7% we observe first sign of Regime I–II transition with the positive deviation from linearity. When the temperature is increased to 95 °C, the photoelastic glassy behavior disappears at all stretch rates, even ones as high as 1000%/min. All stretching rates collapse on to same Regime I classical stress optical behavior and show positive slope change into Regime II indicative of stress crystallization.

A similar trend is observed at 100 °C, with a disappearance of Regime II behavior at the very low rate of 6.7%/min. However, at this condition the slope of the Regime II is highest at 333%/min., due to the fact that relaxation behavior is still prominent at 67%/min even though Regime II exists. For all applied temperatures and stretch rates on HPA6, the Regime I slope remained constant at 2.7 GPa^{-1}.

A remarkable feature of the stress optical graphs for HPA6 is that at all conditions where photoelastic glassy behavior is observed, there is an absence of Regime II behavior. According to the T_{II} concept proposed by Boyer and others [23–26], the amorphous chains exhibit segmental correlations between T_g and T_{II}, and beyond the T_{II} melting of the segments take place leading to formation of true fluid. These segmental correlations enhance the network connectivity and thus act to suppress the relaxation during deformation. Increasing temperature and decreasing rates tend to eliminate this effect.

Fig. 13 displays the strain rate vs. time at various rubbery-state temperatures for HPA6 stretched at 67%/min. The results show that the strain rate at the midsection of the sample is not constant, even though the crosshead separation speed remains the same. From the very beginning of the stretching process, strain rate rises sharply due to highly localized start of deformation at mid symmetry plane of the sample where the measurements are made. The strain rate results can be correlated with the birefringence changes over time in the material, as Fig. 13 depicts. At the start of deformation, both the birefringence and the strain rate increase with time, with the sharpest increases occurring at 80 °C, which is very close to the glass transition temperature. In fact, at 80 °C, the strain rate starts at almost zero value and peaks earlier than samples that are stretched at higher temperatures. The strain rate rapidly reaches a maximum and starts decreasing again, while the birefringence is still increasing sharply. At longer times birefringence begins to level off as the strain rate approaches zero. The increase of stretching temperature increases the time at which the maximum strain rate is observed. Another important observation in Fig. 13 is that the peak position of the strain rate strongly depends upon temperature, moving to longer times as the temperature increases.

Fig. 14 shows a comparison between the structural evolutions of HPA6 material stretched at 6.7%/min and 333%/min, at a temperature of 90 °C. As shown by the WAXD images on the birefringence vs. stress plots, at both stretch rates HPA6 remains essentially amorphous in the beginning stages of the deformation. Only at the end of the Regime I do moderate levels of orientation in the amorphous state develop as indicated by increase equatorial intensity. When the 6.7%/min stretched HPA6 material goes into the Regime II, the appearance of sharp equatorial diffraction spots and weaker off-equatorial spots emerges 0.5 MXD6 typically crystallizes into a triclinic unit cell. (a = 1.201 nm, b = 0.483 nm, c = 2.98 nm, and fiber axis angles of $\alpha = 75.0°$, $\beta = 26.0°$, and $\gamma = 65.0°$) [2]. The partial local chain relaxation coupled with chain orientation during the deformation process at this high temperature (higher fluidity) and low stretch rate (longer time) condition

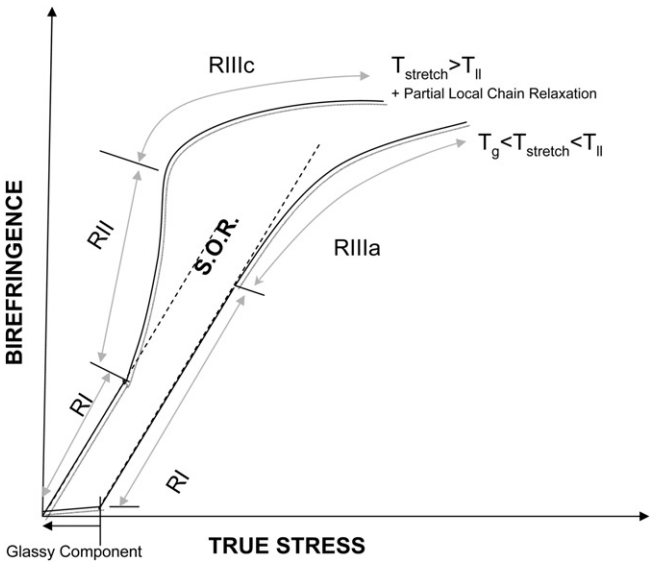

Fig. 9. Generalized stress optical behavior for the deformation of slow crystallizing materials.

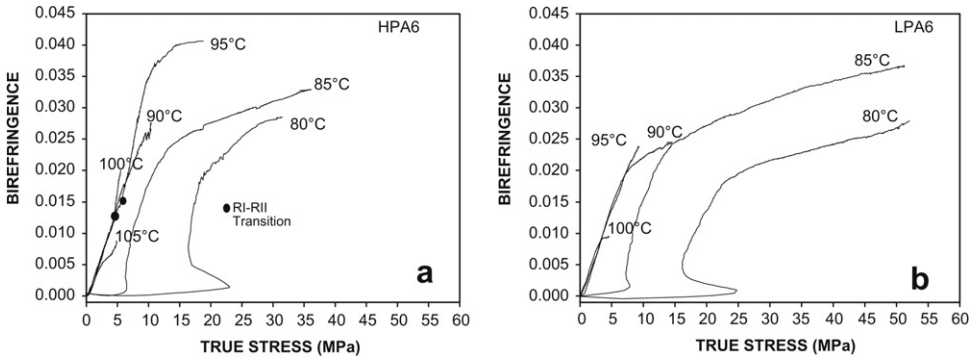

Fig. 10. Stress optical behavior of (a) HPA6 and (b) LPA6 as influenced by temperature, when stretched in the rubbery state at 66.7%/min.

allows the chains to register into crystallographic lattice planes. For samples stretched at 333%/min however, the Regime II is absent and oriented amorphous phase developed within the Regime IIIa as indicated by the darkening of the equatorial spot with higher birefringence levels. These images imply that under conditions where the Regime II is present, oriented crystallization with 3D order occurs, whereas when Regime II is absent, oriented amorphous phase remains.

3.5.1.2. LPA6. The stress optical behavior of LPA6 stretched at 90 °C to a 6× stretch ratio at various rates is depicted in Fig. 15. Just as in HPA6, a photoelastic glassy behavior is evident and it disappears at very low stretch rates (6.7%/min). At this condition we also see a faint evidence of strain crystallization with the appearance of off-equatorial peak at the end of stretching. In this polymer, Regime II behavior is absent for higher stretching rates where Regime I–IIIa behavior is witnessed at all conditions. A very high degree of birefringence is achieved at 667%/min, as the efficiency to orient the polymer chains is very high at this condition where relaxation is highly suppressed. WAXD data taken at the end of stretching shows that at all these conditions where Regime I–IIIa behavior exists, an oriented amorphous structure showing little to no translational order exists at the higher rates, while a highly oriented and 2D ordered structure is present at lower stretch rates, where chain relaxation alongside orientation processes is enhanced.

3.5.2. Strain-optical behavior

Fig. 16 displays where the WAXD tests were taken on the strain-optical curves for HPA6 stretched at 90 °C at different rates of 6.7%/min and 333%/min. The dashed lines on the graph are positioned at the same Hencky strains for both stretch rate conditions, where the structural behavior should be compared. When the material is deformed at 6.7%/min, the strain-optical plot starts becoming highly non-linear and SIC begins to develop at the same birefringence level corresponding to the transition from Regime I to Regime II behavior on the stress optical plot. When deformation occurs at 333%/min, no sharp rise of birefringence with increasing strain is observed on the strain-optical plot and the material remains oriented amorphous even at the end of deformation.

3.6. Effect of molecular weight

3.6.1. Stress optical behavior

Fig. 17 shows a comparison between the structural evolutions in LPA6 and HPA6 material stretched at 90 °C and 6.7%/min. For HPA6, the birefringence increases at a faster rate with stress past the Regime I, and unlike in LPA6, a Regime II behavior is present indicating a higher efficiency to orient and strain crystallize the polymeric chains in HPA6 as a result of the higher chain entanglement density. It is of importance to note that the slope of the Regime I (i.e. the SOC) is not affected by the material molecular weight, as can be observed from the true stress optical behavior.

As shown by the WAXD images on the birefringence vs. stress plots, both M.W. materials remain essentially amorphous in following linear stress optical rule in Regime I. Only at the end of the Regime I do moderate levels of orientation in the amorphous state develop as indicated by the higher concentrations of equatorial intensities in the azimuthal spreads. As the HPA6 material goes into the Regime II, the appearance of sharp equatorial diffraction spots and weaker off-equatorial spots emerges at a Hencky strain value of 1.71 and crystal order is enhanced by further stretching to 1.74 Hencky strain as indicated by the

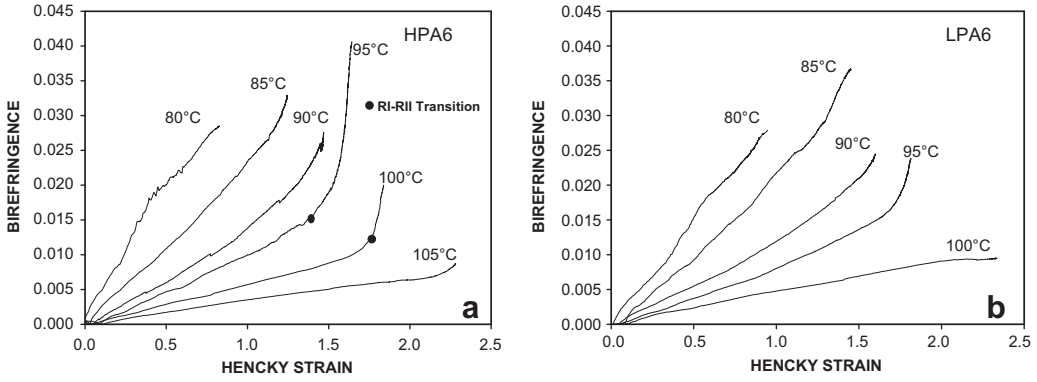

Fig. 11. Strain-optical behavior of (a) HPA6 and (b) LPA6 as influenced by temperature, when stretched in the rubbery state at 66.7%/min.

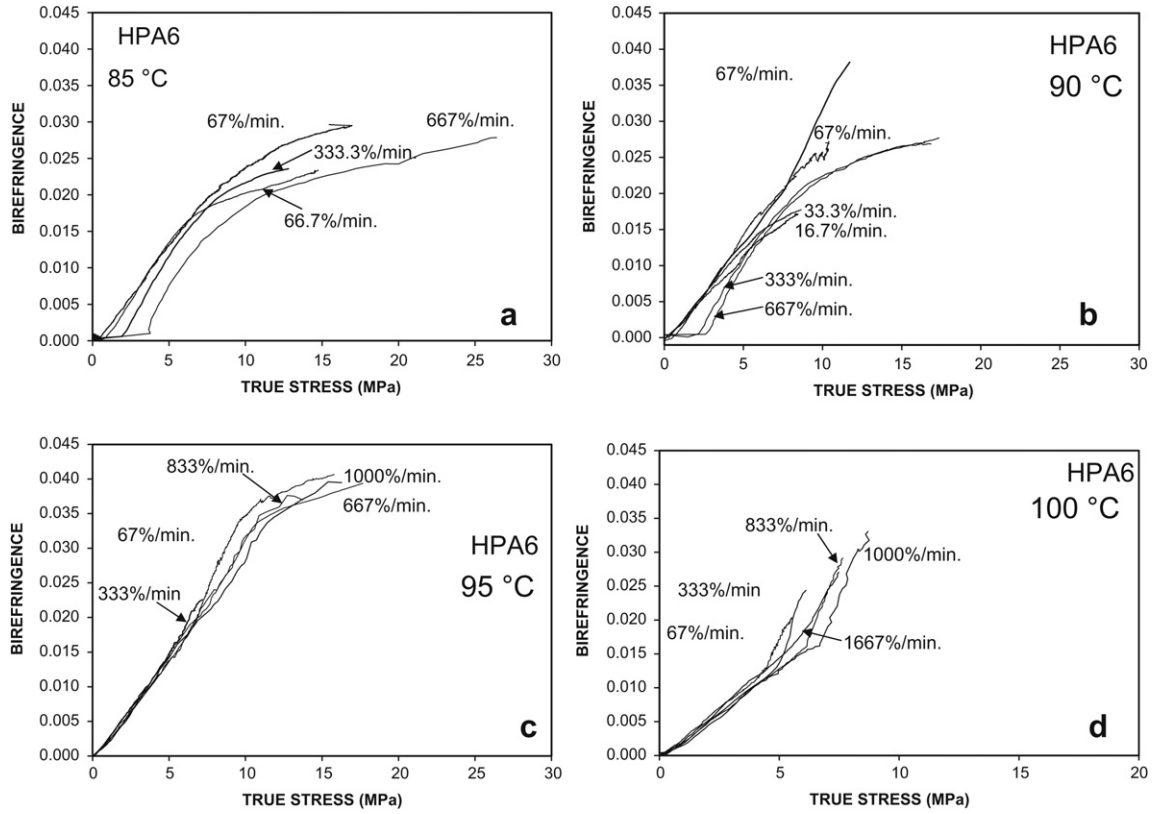

Fig. 12. Stress optical behavior of HPA6 as influenced by stretch rate, when stretched in the rubbery region at (a)85 °C (b) 90 °C (c) 95 °C and (d)100 °C.

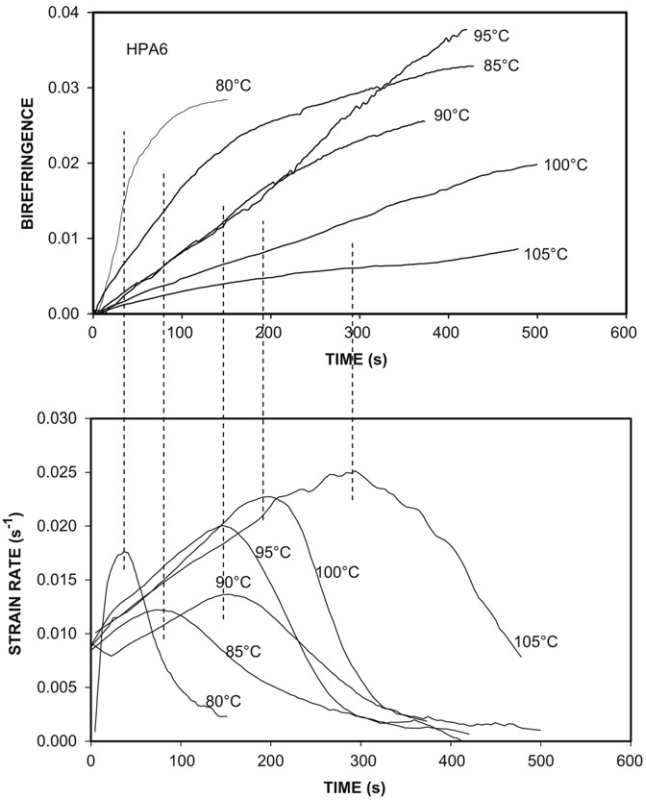

Fig. 13. Change of birefringence with time (top) and change of strain rate with time (bottom) for HPA6 stretched at several temperatures and a rate of 66.7% min.

sharpening of these spots. Off-equatorial peaks are not present in LPA6 material that's stretched to the highest Hencky strain level reached in HPA6. In fact, even at 1.74 Hencky strain the lower molecular weight material shows only weak equatorial spots, implying a poorly oriented and ordered structure is formed. Only when this low M.W. polymer is stretched to a very high Hencky strain value of 1.79 does a sharp crystallographic peak forms, implying the presence of a highly oriented and 2D ordered structure lacking 3D translational crystal order as indicated by the absence of off-equatorial diffraction spots.

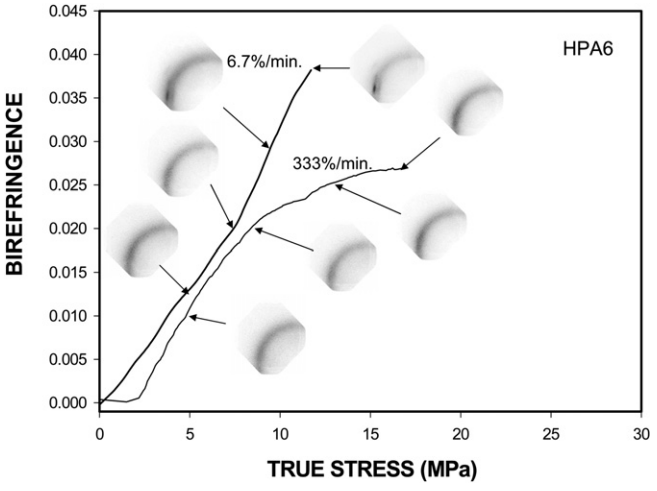

Fig. 14. Comparison between the structural evolutions of HPA6 material stretched at 6.7%/min and 333%/min, at a temperature of 90 °C.

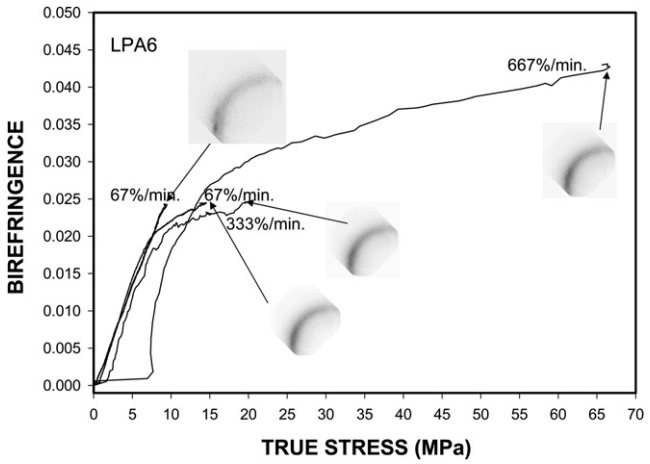

Fig. 15. Stress optical behavior of LPA6 stretched at 90 °C to a 6× stretch ratio at various rates.

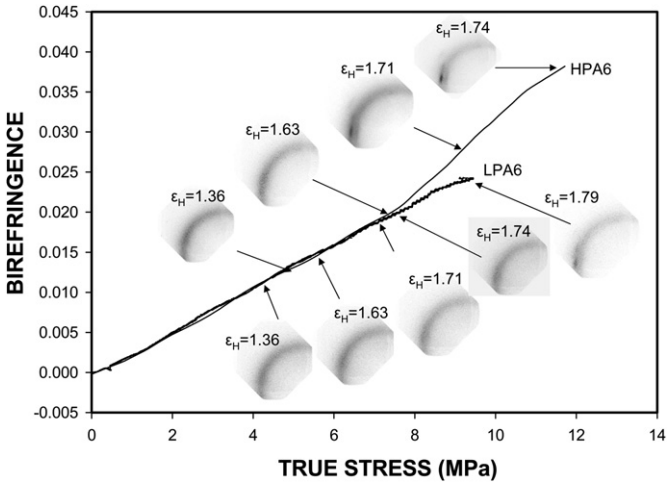

Fig. 17. M.W. effect on the structural evolutions of Nylon MXD6 film stretched at 90 °C and 6.7%/min.

It is of importance to note that even for HPA6, the off-equatorial diffraction spots are not very sharp as compared to materials like PLA [7] that show much brighter diffraction spots early on in the Regime II, indicating that the relatively low M.W. of Nylon MXD6 as compared to material like PLA results in lower amorphous orientation and crystallinity when strain is applied due to lower entanglement density exhibited by MXD6.

3.6.2. T_{II} studies

When the slopes of the glassy components, known otherwise as photoelastic constants (PEC), for LPA6 and HPA6 stretched at 66.7%/min are plotted against temperatures ranging from just above glass transition temperature to temperatures just before thermal crystallization (<110 °C) (see Fig. 18), an increase in the slopes with temperature is observed until the glassy component disappears and the photoelastic constant becomes equal to the stress optical constant (SOC), which is the slope of the Regime I. Beyond the critical temperature at which this happens, known as the T_{II}, the slope remains constant and material attains true "unstructured" fluid state. In general, the SOC was found to decrease with increasing temperature for both M.W. grades, reaching a constant value past T_{II}. For LPA6, the T_{II} was observed at approximately 1.26 × T_g while for HPA6, it was observed at approximately 1.20 × T_g.

Fig. 19 shows that both stress optical as well as photoelastic constants are independent of molecular weight. Beyond the value of T_{II}, which is 95 °C, true fluid behavior is attained whereby the stress optical constant becomes truly independent of temperature and rate (see also Fig. 15). In addition, the stress optical constant (SOC) was about the same for both M.W. materials stretched at temperatures past T_{II}, at 2.7 GPa^{-1} for HPA6 and 2.61 GPa^{-1} for LPA6.

3.7. Molecular model

Fig. 19 displays a conceptual molecular model for the uniaxial deformation of Nylon MXD6 at conditions which favor strain crystallizability, when high M.W. in conjunction with either medium high temperatures (90 °C) and lower rates (6.7%/min) or high temperatures (95 °C and higher) and higher rates are applied. The first diagram depicts the material in the as-cast amorphous state, in which it possesses several entangled clusters with the chains being randomly oriented throughout the film. As the deformation proceeds, the polymer chains become well oriented and due to partial chain relaxation crystallize, with the highly

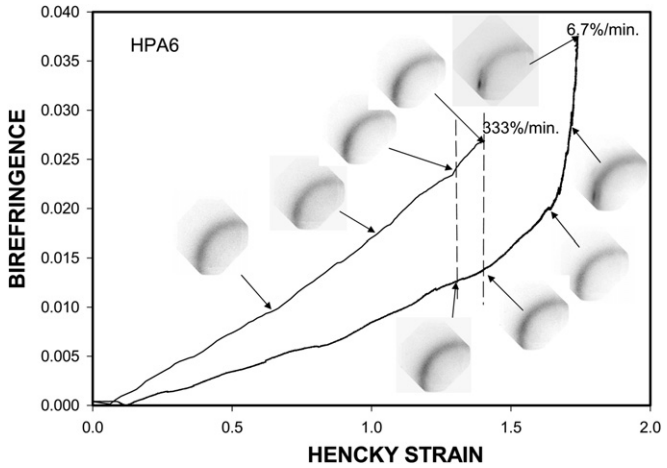

Fig. 16. Comparison between the structural evolutions of HPA6 material stretched at 6.7%/min and 333%/min, at a temperature of 90 °C: strain-optical plots.

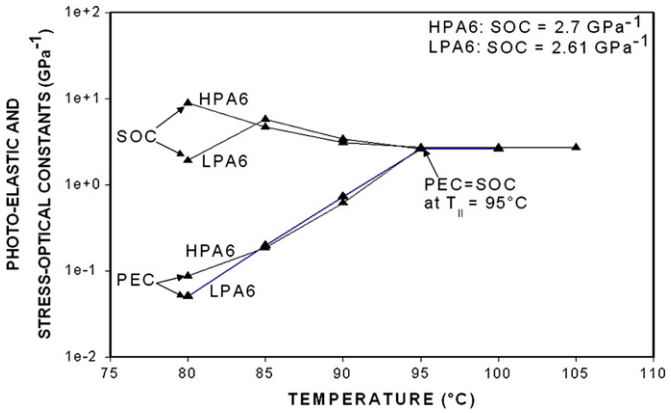

Fig. 18. Photo-elastic constant and stress-optical constant versus temperature for LPA6 and HPA6 stretched at 66.7%/min.

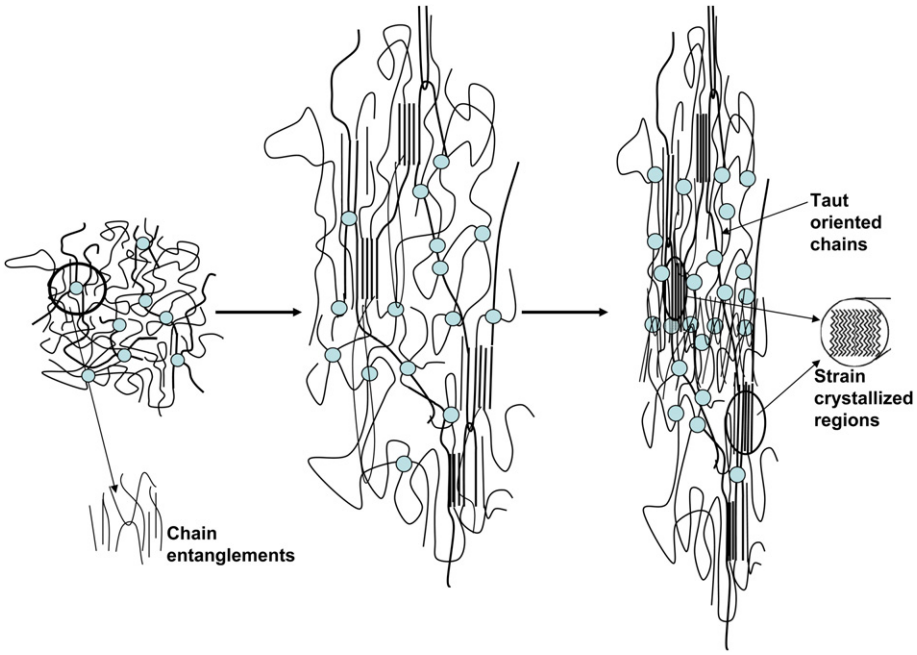

Fig. 19. Molecular model of different stages of the rubbery state deformation of high M.W. Nylon MXD6 film showing chain entanglements and strain crystallized regions.

oriented adjacent chains registering themselves into the crystal lattice formation. A physical network is formed consisting of both entanglement junctions as well as crystallite nodes that act as additional "crosslinking" junctions. Together, they pull the chains between them in the deformation direction until they become highly oriented and taut, resulting in a very rapid rise in oriented crystallization. The entangled clusters, as well as the crystallite nodes, eventually become positioned side-by-side in the film transverse direction, dramatically slowing down TD contraction at large deformation levels.

4. Conclusions

In this paper, the influence of temperature, rate, and molecular weight on large deformation stress optical behavior, strain-optical behavior and Poisson's ratio changes of Nylon MXD6 films deformed uniaxially in the rubbery state from amorphous precursors were mapped out. For all M.W. Nylon MXD6, deformation between T_g and T_{ll} resulted in an initial glassy response whereby the polymer exhibited photoelastic behavior and remained amorphous. This glassy response diminished with higher temperatures and/or lower rates, until totally disappearing at 95 °C for all employed rates. This photoelastic behavior was followed by a Regime I–IIIa behavior, where the birefringence rises linearly at a much faster rate with true stress (Regime I) before approaching a plateau behavior (Regime IIIa). Even at the end of the Regime IIIa, the material remained in the oriented amorphous state. When high M.W. in conjunction with higher temperatures and/or lower rates was used, a Regime I–II–IIIc behavior was evident and a constrained 3D crystal structure was formed. It was also found that a change in molecular weight did not significantly alter the values of photoelastic constant (PEC) at the different test temperatures or the value of the liquid–liquid transition T_{ll}, which was found to be equal to 95 °C. In addition, the stress optical constant (SOC) was about the same for both M.W. materials stretched at temperatures past T_{ll}, at 2.7 GPa^{-1} for HPA6 and 2.61 GPa^{-1} for LPA6.

Acknowledgment

We would like to thank Dr. Doug Callander for providing the Nylon MXD6 pellets needed to cast film sheets.

References

[1] Umemura J, Murata Y, Tsunashima K, Koizumi N. Journal of Polymer Science: Part B: Polymer Physics 1999;37:531–8.
[2] http://www.mgc-a.com/Pages/MXD6/hist-mxd6.html.
[3] http://www.gasbarriertechnologies.com/ds_process.html.
[4] http://www.mgc-a.com/Pages/MXD6/bottle.html.
[5] http://www.gasbarriertechnologies.com/ds_various.html.
[6] Prattipati V, Hu YS, Bandi S, Schiraldi DA, Hiltner A, Baer E, et al. Journal of Applied Polymer Science 2005;97:1361–70.
[7] Mulligan JH, Cakmak M. Macromolecules 2005;38:2333–44.
[8] Martins CI, Cakmak M. Macromolecules 2005;38:4260–73.
[9] Drinan. J, Prentice, Stanaszek, Straker. SPE ANTEC 2000 Conference Proceedings: CRC Press; 2000 3728–30.
[10] Olabisi O. Handbook of thermoplastics. CRC Press; 1997. p. 941.
[11] Martins CI, Cakmak M. Polymer 2007;28:2109–23.
[12] Day M, Nawaby AV, Liao X. Journal of Thermal Analysis and Calorimetry 2006;86(3):623–9.
[13] Dai X, Luo X, Gu Q, Zhang X, Shen D, Shi L, et al. Chinese Journal of Polymer Science 2002;20(5):481–3.
[14] Janeschitz-Kriegl H. Polymer melt rheology and flow birefringence. Berlin: Springer-Verlag; 1983. p. 552.
[15] Reiss-Nunes RC, Riande E, Guzman J, Chavez NA. Macromolecules 2000;33:9464–7.
[16] Salem DR. Polymer 1992;33:3182–8.
[17] Stein RS. Polym. Eng. Sci. 1976;16:152–7.
[18] Inoue T, Ryu DS, Osaki K. Macromolecules 1998;31:6977–83.
[19] Kroeger M, Luap C, Muller R. Macromolecules 1997;30:526–39.
[20] Matsumoto T, Bogue DC. J. Polym. Sci. Phys. 1977;15:1663–74.
[21] Inoue T, Okamoto H, Osaki K. Macromolecules 1991;24:5670–5.
[22] Inoue T, Osaki K. Macromolecules 1996;29:1595–9.
[23] Murthy SSN. Journal of Polymer Science Part B: Polymer Physics 2003;31(4):475–80.
[24] Boyer RF. Order in the amorphous "state" of polymers. New York: Plenum Press; 1987. pp. 135–85.
[25] Lobanov AM, Frenkel SY. Polymer Science USSR 1980;22:1150.
[26] Boyer RF. J. Polym. Sci. Polym. Phys. 1988;26:893.
[27] Lakes RS. Cellular Polymers 1992;11:466–9.
[28] Tschoegl NW, Knauss WG, Emri I. Mechanics of Time-Dependent Materials 2002;6:3–51.
[29] Choi JB, Lakes RSJ. Materials Science 1992;27:4678–84.
[30] Wilson I, Ladizesky NH, Ward IM. Journal of Materials Science 1976;11:2177–80.

[31] Kugler. H.P, Stacer. R.G, Steimle. C. "Direct measurement of Poisson's ratio in elastomers" ACS Meeting; 1989 473–87
[32] Ma T, Bhushan B, Murooka H, Kobayashi L, Osawa T. Review of Scientific Instruments 2002;73(4):1813–20.
[33] Smith TL. Transaction of the Society of Rheology 1959;3:113–36.
[34] Valladares D, Toki S, Sen TZ, Yalcin B, Cakmak M. Macromolecular. Symposia. 2002;185:149–66.
[35] Koike Y, Cakmak M. Polymer 2003;44:4249–60.
[36] Kwa. T.L. Masters thesis. University of Akron, Akron, OH, USA; 2006
[37] Kanuga K, Cakmak M. Polymer 2007;48:7176–92.